Two-dimensional model of low Mach number vortex sound generation in a lined duct

S. K. Tang[a] and C. K. Lau[b]

Department of Building Services Engineering, The Hong Kong Polytechnic University, Hong Kong, China

The sound generated by a vortex moving across a duct section lined with porous materials and the corresponding vortex dynamics are studied numerically in the present investigation. The combined effects of the effective fluid density, the flow resistance, the length, and the thickness of the porous linings on the vortex dynamics and sound generation are examined in detail. Results show that stronger sound radiation will take place when the length and the thickness of the porous linings are increased or when the effective fluid density is reduced. The flow resistance can only result in stronger sound radiation within a range whose width depends on the abovementioned system parameters. Such sound amplification cannot be achieved when the initial vortex height gets closer and closer to the duct centerline. The present results also indicate the strong correlation between vortex acceleration and the sound radiation under the actions of the porous linings.
© 2009 Acoustical Society of America. [DOI: 10.1121/1.3192332]

I. INTRODUCTION

Commercial buildings in a sub-topical city nowadays are very heavily serviced. A significant portion of the noise inside these buildings comes from the air conditioning and ventilation systems. The low Mach number turbulent flows inside the ductwork are also sound producing, especially when they interact with obstacles.[1,2] These aerodynamic noises are of low frequency and they propagate into the occupancy zones together with the system noises through the ductwork.

In order to achieve a reasonable level of indoor noise, dissipative silencers and acoustical linings,[3] which consist of porous materials like fiberglass, are commonly used to attenuate the system noise before it reaches the occupancy zones. There are studies on modeling the sound attenuation by dissipative silencers in the presence of a mean flow (for instance, Cummings and Chang[4] and Peat and Rathi[5]) and on the design of high attenuation silencers (for instance, Selamat *et al.*[6]). However, there are evidences showing that the low Mach number turbulent flow can interact with an absorbent liner to produce sound.[7,8] The low frequency characteristic of this noise makes it very difficult to attenuate by conventional methods. It is therefore important to study how this aerodynamic noise will reduce the performance of dissipative silencers and the wall linings.

Flow turbulence is very difficult to model analytically. However, the low Mach number flow condition inside the building air ductwork makes it possible to model the turbulent eddies as discrete vortices moving in an incompressible flow, which can then be handled analytically by the potential theory.[9] Once the motions of the vortices are obtained, the vortex sound theory[10] can basically be used to estimate the vortex sound so generated. Though the vortex is a drastic simplification of the flow turbulence, this semi-analytical approach has attracted the attention of many researchers as it is expected that this vortex analogy can provide insights into the aeroacoustics of more complicated low Mach number turbulent flows. Typical examples include the works of Cannell and Ffowcs Williams,[11] Crighton,[12] and Obermeier.[13] More examples can be found in Ref. 14.

Many of the works in the existing literature deal with vortex sound in the presence of a rigid boundary. Recently, Tang[15] worked out the vortex dynamics in the presence of porous surfaces. The authors have also extended the vortex sound study to include the porous wedge and cylinder.[16,17] Lau and Tang[17] showed that the dipole sound generation under the effect of the porous cylinder can be stronger than that generated in the presence of a rigid cylinder. The more recent work of the authors examines the vortex sound radiation under the influence of a porous lining in an opened space.[18]

In the present investigation, the vortex sound generation inside an infinitely long two-dimensional rigid wall duct with porous linings of finite length on both sides of the duct is studied. This configuration is analogous to the situation of a lined duct in the air conditioning and ventilation ductwork. It is hoped that the present study could enhance the general understanding on vortex sound generation and be able to provide insights for further development of aeroacoustic modeling of wall linings and dissipative silencers.

II. THEORETICAL DEVELOPMENT

Figure 1 illustrates the schematics and the essential nomenclature adopted in the present study. An inviscid vortex initially at a distance very far away from the porous materials propagates toward the latter under the effect of the rigid duct walls in an incompressible fluid medium. Crighton[12] showed explicitly that the near field incompressible solution can be

---

[a] Author to whom correspondence should be addressed. Electronic mail: besktang@polyu.edu.hk

[b] Present address: Ove Arup & Partners, Level 5, Festival Walk, Kowloon, Hong Kong, People's Republic of China.
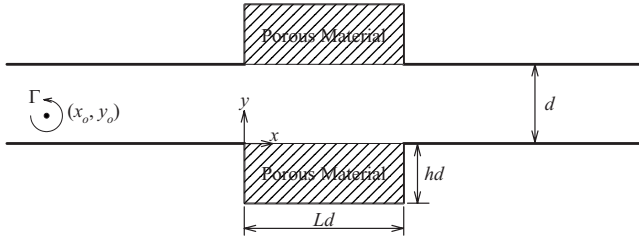
FIG. 1. Schematic of the vortex-lined duct system.

used to estimate the far field acoustic radiation through a matching technique in the low Mach number condition. This is also the approach adopted in the present study.

All length scales in the present study are normalized using the width of the duct d. The time and velocities are normalized by d^2/Γ and Γ/d, respectively. As in the previous studies of the authors,[15–18] the air density inside the duct is denoted by ρ while the properties of the porous materials are characterized using the effective density ρ_e and the flow resistance R_f inside its lattice.[19] The flow resistance is normalized by $\rho\Gamma/d^2$. Under the low Mach number condition, the flow inside the porous material, which is expected to be very weak, is incompressible. To simplify the analysis, the porous material is assumed to be a continuum and thus the potential theory applies.

Denoting the streamfunctions within the duct ($0 \leq y \leq 1$), in the upper porous layer ($1 \leq y \leq 1+h, 0 \leq x \leq L$), and in the lower porous layer ($-h \leq y \leq 0, 0 \leq x \leq L$) as ψ, ψ_{pu}, and ψ_{pl}, respectively, one finds that

$$\nabla^2 \psi = -\delta(x - x_o)\delta(y - y_o), \qquad (1)$$

and

$$\nabla^2 \psi_{pu} = \nabla^2 \psi_{pl} = 0, \qquad (2)$$

where ∇^2 and δ are the Laplacian operator and delta function, respectively. Since the normal fluid velocities at the interfaces between the porous material and the rigid walls vanish, one observes that

$$\left. \frac{\partial \phi_{pl}}{\partial x} \right|_{x=0} = \left. \frac{\partial \psi_{pl}}{\partial y} \right|_{x=0} = \left. \frac{\partial \phi_{pl}}{\partial x} \right|_{x=L} = \left. \frac{\partial \psi_{pl}}{\partial y} \right|_{x=L}$$
$$= -\left. \frac{\partial \psi_{pl}}{\partial x} \right|_{y=-h} = 0, \qquad (3)$$

and

$$\left. \frac{\partial \phi_{pu}}{\partial x} \right|_{x=0} = \left. \frac{\partial \psi_{u}}{\partial y} \right|_{x=0} = \left. \frac{\partial \phi_{pu}}{\partial x} \right|_{x=L} = \left. \frac{\partial \psi_{pu}}{\partial y} \right|_{x=L}$$
$$= -\left. \frac{\partial \psi_{pu}}{\partial x} \right|_{y=1+h} = 0, \qquad (4)$$

where ϕ_{pl} and ϕ_{pu} denote the flow potentials within the lower and upper porous layers, respectively. It is straightforward to show from Eqs. (2)–(4) that

$$\psi_{pl} = \sum_{n=1}^{\infty} A_n e^{\alpha_n h} \sin(\alpha_n x) \sinh[\alpha_n(h + y)], \qquad (5)$$

and

$$\psi_{pu} = \sum_{n=1}^{\infty} B_n e^{\alpha_n(1+h)} \sin(\alpha_n x)\sinh[\alpha_n(1 + h - y)], \qquad (6)$$

where n is a non-zero integer, $\alpha_n = n\pi/L$, and A_n and B_n the mode magnitudes. The Fourier transform with respect to x of Eq. (1) gives

$$\Psi = \int_{-\infty}^{\infty} \psi e^{ikx} dk = \begin{cases} G_1 e^{-|k|y} + G_2 e^{|k|y}, & 0 \leq y \leq y_o \\ H_1 e^{-|k|y} + H_2 e^{|k|y}, & y_o \leq y \leq 1, \end{cases} \qquad (7)$$

where G_1, G_2, H_1, and H_2 are functions of k. The continuity of Ψ and the vorticity jump $\partial\Psi/\partial y$ at $y = y_o$ lead to

$$H_1 - G_1 = \frac{1}{2|k|} e^{ikx_o + |k|y_o} \text{ and } G_2 - H_2 = \frac{1}{2|k|} e^{ikx_o - |k|y_o}. \qquad (8)$$

The continuity of normal fluid velocity at the porous layer surface at $y = 0$, $0 \leq x \leq L$ gives

$$-\left. \frac{\partial \psi}{\partial x} \right|_{y=0} = -\left. \frac{\partial \psi_{pl}}{\partial x} \right|_{y=0} \Rightarrow \Psi|_{y=0} = \Psi_{pl}|_{y=0}. \qquad (9)$$

The same condition at the upper porous layer surface at $y = 1$, $0 \leq x \leq L$ gives

$$\Psi|_{y=1} = \Psi_{pu}|_{y=1}. \qquad (10)$$

It follows from Eqs. (9) and (10) that

$$G_1 = \sum_{n=1}^{\infty} \alpha_n A_n e^{\alpha_n h} \sinh(\alpha_n h) \frac{(-1)^n e^{ikL} - 1}{k^2 - \alpha_n^2} - G_2, \qquad (11)$$

and

$$H_1 = \sum_{n=1}^{\infty} \alpha_n B_n e^{\alpha_n(1+h)} \sinh(\alpha_n h) \frac{(-1)^n e^{ikL} - 1}{k^2 - \alpha_n^2} e^{|k|}$$
$$- H_2 e^{2|k|}. \qquad (12)$$

G_1, G_2, H_1, and H_2 can thus be obtained in terms of the mode magnitudes α_n, h, L, and k by solving Eqs. (8), (11), and (12) together and are shown in the Appendix. It can then be shown with the use of Eq. (7) that

$$\Psi = \frac{e^{ikx_o}\sinh(|k|y)\sinh(|k|(1-y_o))}{|k|\sinh(|k|)}$$

$$+ \frac{1}{\sinh(|k|)}\sum_{n=1}^{\infty}\left\{\alpha_n e^{\alpha_n h}\sinh(\alpha_n h)\frac{(-1)^n e^{ikL}-1}{k^2-\alpha_n^2}[A_n\sinh(|k|(1-y))+e^{\alpha_n}B_n\sinh(|k|y)]\right\}. \quad (13)$$

Following the previous study of the authors,[15,18] the vortex velocities are

$$\dot{x}_o = \frac{1}{2\pi}\int_{-\infty}^{\infty}\frac{\partial}{\partial y}\left(\Psi - \frac{1}{2|k|}\exp(ikx_o+|k|y)\right.$$

$$\left.-|k|y_o\right)e^{-ikx}dk\bigg|_{x=x_o,y=y_o}$$

$$= \frac{1}{4}\cot(\pi y_o) - \sum_{n=1}^{\infty}\alpha_n e^{\alpha_n h}\sinh(\alpha_n h)$$

$$\times\int_0^{\infty}\frac{(-1)^n\cos[k(L-x_o)]-\cos(kx_o)}{\pi(k^2-\alpha_n^2)\sinh(k)/k}$$

$$\times(A_n\cosh[k(1-y_o)]-B_n e^{\alpha_n}\cosh(ky_o))dk \quad (14)$$

and

$$\dot{y}_o = -\frac{1}{2\pi}\int_{-\infty}^{\infty}\frac{\partial}{\partial x}\left(\Psi - \frac{1}{2|k|}\exp(ikx_o+|k|y)\right.$$

$$\left.-|k|y_o\right)e^{-ikx}dk\bigg|_{x=x_o,y=y_o}$$

$$= -\sum_{n=1}^{\infty}\alpha_n e^{\alpha_n h}\sinh(\alpha_n h)$$

$$\times\int_0^{\infty}\frac{(-1)^n\sin[k(L-x_o)]+\sin(kx_o)}{\pi(k^2-\alpha_n^2)\sinh(k)/k}$$

$$\times(A_n\sinh[k(1-y_o)]+B_n e^{\alpha_n}\sinh(ky_o))dk, \quad (15)$$

where use has been made of the formulas given by Gradshteyn and Ryzhik[20] and "·" denotes time differentiation. The continuity of pressure at the porous layer surfaces requires that

$$\frac{\partial}{\partial t}\left(\frac{\partial\psi}{\partial y}\bigg|_{y=0}\right) = \eta\frac{\partial}{\partial t}\left(\frac{\partial\psi_{pl}}{\partial y}\bigg|_{y=0}\right) + R_f\frac{\partial\psi_{pl}}{\partial y}\bigg|_{y=0} \quad \text{and}$$

$$\frac{\partial}{\partial t}\left(\frac{\partial\psi}{\partial y}\bigg|_{y=1}\right) = \eta\frac{\partial}{\partial t}\left(\frac{\partial\psi_{pu}}{\partial y}\bigg|_{y=1}\right) + R_f\frac{\partial\psi_{pu}}{\partial y}\bigg|_{y=1}, \quad (16)$$

where $\eta=\rho_e/\rho$. The application of inverse Fourier transform of Eq. (7) suggests that

$$\frac{1}{2\pi}\int_{-\infty}^{\infty}|k|(\dot{G}_2-\dot{G}_1)e^{-ikx}dk$$

$$= \sum_{n=1}^{\infty}(\eta\dot{A}_n+R_fA_n)\alpha_n e^{\alpha_n h}\sin(\alpha_n x)\cosh(\alpha_n h), \quad (17)$$

and

$$\frac{1}{2\pi}\int_{-\infty}^{\infty}|k|(\dot{H}_2 e^{|k|}-\dot{H}_1 e^{-|k|})e^{-ikx}dk$$

$$= -\sum_{n=1}^{\infty}(\eta\dot{B}_n+R_fB_n)\alpha_n e^{\alpha_n(1+h)}\sin(\alpha_n x)\cosh(\alpha_n h). \quad (18)$$

Using the technique of Lau and Tang,[18] the rates of change in the mode magnitudes and the vortex velocities can be estimated from their instantaneous values by solving the simultaneous equations [Eqs. (14), (15), (17), and (18)] with the initial condition $\dot{A}_n=\dot{B}_n=0$, $\dot{y}_o=0$, and $\dot{x}_o=\cot(\pi y_o)/4$. The position of the vortex as well as the mode magnitudes can then be estimated using standard Runge–Kutta method as in the previous study of the authors.[18]

The flow potential due to the presence of the vortex can be found by applying the Cauchy–Rieman principle,[21] which states that

$$\frac{\partial\psi}{\partial y} = \frac{\partial\phi}{\partial x} \Rightarrow \phi = \frac{1}{2\pi}\int_{-\infty}^{\infty}\frac{i}{k}\frac{\partial\Psi}{\partial y}e^{-ikx}dk + C, \quad (19)$$

where C is a spatial invariant, but may vary with time.

$$\phi = \frac{1}{2\pi}\tan^{-1}\left[\tan\left(\frac{(1-y_o+y)\pi}{2}\right)\tanh\left(\frac{(x-x_o)\pi}{2}\right)\right]$$

$$+ \frac{1}{2\pi}\tan^{-1}\left[\tan\left(\frac{(1-y_o-y)\pi}{2}\right)\tanh\left(\frac{(x-x_o)\pi}{2}\right)\right]$$

$$+ \frac{1}{\pi}\sum_{n=1}^{\infty}\alpha_n e^{\alpha_n h}\sinh(\alpha_n h)$$

$$\times\int_0^{\infty}\frac{(-1)^{n+1}\sin[k(x-L)]+\sin(kx)}{k^2-\alpha_n^2}$$

$$\times\frac{A_n\cosh[k(1-y)]-B_n e^{\alpha_n}\cosh(ky)}{\sinh(k)}dk + C. \quad (20)$$

The summation term in Eq. (20) represents the vortex potential induced by fluid motions at the surface of the porous material, while those with the arctangent the vortex potential for infinitely long rigid duct. It can be observed that

$$(\phi - C)|_{x \to \infty} = - \ (\phi - C)|_{x \to -\infty} \Rightarrow (\dot{\phi} - \dot{C})|_{x \to \infty}$$

$$= - \ (\dot{\phi} - \dot{C})|_{x \to -\infty} \quad (21)$$

and

$$\partial \phi / \partial x|_{x \to \infty} = \ \partial \phi / \partial x|_{x \to -\infty}. \quad (22)$$

The general solution of the flow potential at $|x| \to \infty$, where the duct walls are rigid, is

$$\phi_i = \phi + \Omega x, \quad (23)$$

where Ω is a function of time. The low Mach number vortex motion will produce a low frequency plane wave at $|x| \to \infty$,[11] and thus in the leading order at large $|x|$:

$$\frac{1}{c} \frac{\partial \phi_i}{\partial t} = - \mathrm{sgn}(x) \frac{\partial \phi_i}{\partial x}, \quad (24)$$

where c denotes the ambient speed of sound normalized by Γ / d. It can then be concluded from Eqs. (21)–(24) that $\dot{C} \to 0$, implying that C is also a or nearly a time invariant and is not important in the sound generation.

It can be shown using the formula depicted by Gradshteyn and Ryzhik[20] that the vortex potential for $x \to \infty$ is

$$\phi_\infty = \frac{1}{2}(1 - y_o) + \sum_{n=1,3,5,\dots}^{\infty} \left[e^{\alpha_n h}(B_n e^{\alpha_n} - A_n) \frac{\sinh(\alpha_n h)}{\alpha_n} \right]$$

$$+ O(e^{-x}). \quad (25)$$

A plane wave is generated in the far field and thus the far field potential ϕ_0 downstream of the lined duct will take the form of

$$\phi_o = \Lambda \exp(- ikx) \quad (26)$$

in the frequency domain. By applying the technique of matched asymptotic expansion,[22] the low frequency inner solution of the far field potential (at $kx \to 0$) must match with the Fourier transform of ϕ_∞ with respect to time. Therefore

$$\Lambda = \int_{-\infty}^{\infty} \phi_\infty e^{-i\omega t} dt. \quad (27)$$

It follows that the far field pressure as $|x| \to \infty$ is

$$p(x,t) = - \frac{1}{2\pi} \frac{\partial}{\partial t} \int_{-\infty}^{\infty} \mathrm{sgn}(x) \Lambda \exp(- ik|x|) e^{i\omega t} d\omega$$

$$= - \mathrm{sgn}(x) \frac{\partial}{\partial t} \phi_\infty(t - |x|/c). \quad (28)$$

A planar dipole is produced and the far field pressure is normalized by $\rho \Gamma^2 / d^2$.

In the present study, the effect of a low Mach number mean flow inside the duct is not considered. However, it has been shown by Ffowcs Williams and Lovely[23] and more recently by Tang et al.[24] that the mean flow tends to strengthen the overall sound power radiation. It should be noted that the results of Howe[25] show that the mean flow will induce "jetting" effects at the apertures of a perforated plate which eventually causes the vortex to move toward the plate. Such phenomenon is also expected when the perforated plate is replaced by a piece of porous material. One can anticipate that the jetting effect is weaker for porous material because of the damping from the flow resistance in the complicated lattice of the porous material. However, the anticipated slightly higher vortex transverse velocity will result in stronger sound radiation. The present case therefore represents the minimum vortex sound radiation in a lined duct. The effect of mean flow on the duct sound generation is much more complicated and is left for further investigation.

III. RESULTS AND DISCUSSIONS

In the present study, the vortex is located far upstream of the porous materials initially. Therefore, only the cases where the initial height of the vortex y_{oi} is smaller than 0.5 will be considered as the vortex is stationary if $y_{oi} = 0.5$ and will move further upstream if $y_{oi} > 0.5$ in the absence of a mean flow with nearly constant speed and thus radiates no sound. One can also notice that many equations involved infinite summations which have to be truncated in the computation as in many previous studies (for instance, Lau and Tang[18]). It is found that the difference of the far field pressure amplitudes for $y_{oi} = 0.2$, $L = 2$, $h = 0.2$, and $\eta = 3$ with various R_f computed with five-term summation and ten-term summation is within 1%–2%. Thus, five-term summation is adopted in the present computation. The density ratio η in practice is less than 5 according to Morse and Ingard,[19] while the practice range of R_f is discussed by Lau and Tang.[17] In fact, the value of R_f can vary over a wide range. For a perfectly inviscid fluid, $R_f = 0$, but for a nearly rigid material, $R_f \to \infty$.

A. Perfectly inviscid fluid

For a perfectly inviscid fluid, the flow resistance inside the lattice of the porous material vanishes ($R_f = 0$). Figure 2(a) shows the paths of the vortex under different combinations of h and η with L fixed at unity and $y_{oi} = 0.2$. The pressure releasing effect from the lower porous material results in the downward movement of the vortex. The smaller the effective density η or the increase in h strengthens the pressure releasing effect of the porous materials and thus gives rise to deeper downward bend of the vortex path. As in Ref. 18, the paths will become independent of h when h becomes large (not shown here). One can also observe from Fig. 2(a) that the influence of the porous materials becomes significant at $x \sim -1$. Unlike the case of an infinite plate in an unbound fluid medium,[18] the vortex paths in the present lined duct case are not symmetrical about the vertical middle plane of the porous materials ($x = 0.5L$). The vortex attains its minimum height at a location slightly larger than $0.5L$ so that the vortex cannot return to its original height even under the pressure supporting effects of the downstream rigid duct walls. The difference between the original and the final height of the vortex decreases with weaker pressure releasing effect of the porous materials. The vortex therefore propagates with higher speed after moving across the lined section of the duct. Such increase in vortex speed suggests that a net vertical downward force is exerted onto the fluid during such

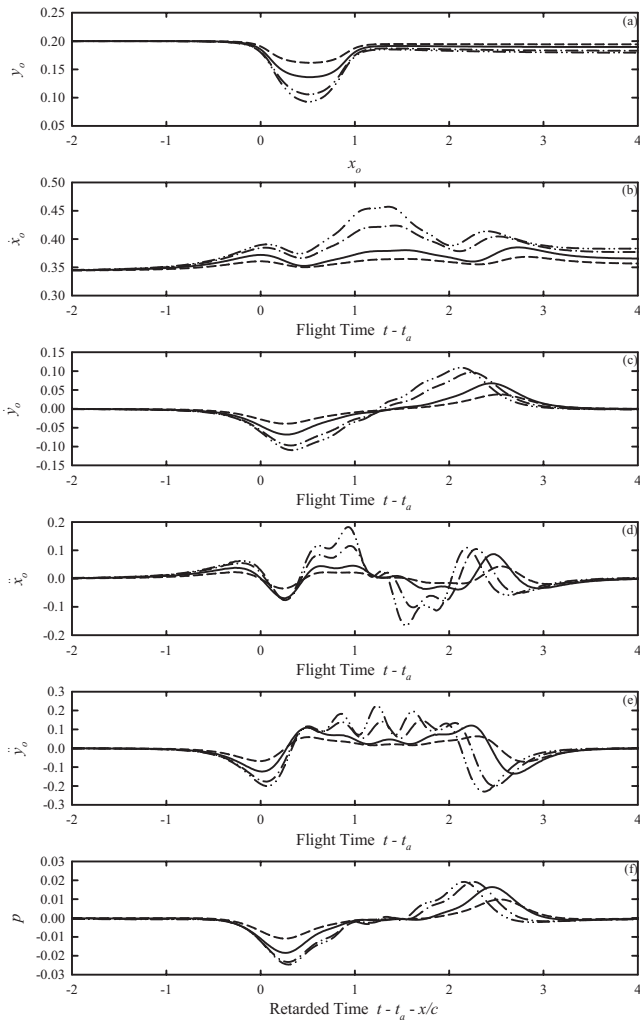S. K. Tang and C. K. Lau: Duct vortex sound

FIG. 2. Effects of pressure-releasing linings on vortex dynamics and sound generation under inviscid condition for $L=1$ and $y_{oi}=0.2$. (a) Vortex path, (b) longitudinal velocity, (c) transverse velocity, (d) longitudinal acceleration, (e) transverse acceleration, and (f) far field sound pressure. ——: $h=0.2$, $\eta=3$; – – –: $h=0.2$, $\eta=5$; –··–: $h=0.4$, $\eta=3$; and –·–·–: $h=0.8$, $\eta=3$.

maneuver of the vortex, which resulted from the difference in the pressure releasing effects between the upper and lower porous linings.

Figures 2(b) and 2(c) illustrate the time variations in the longitudinal and transverse velocities of the vortex during its interaction with the linings. t_a in the figures and hereinafter denotes the time at which the vortex passes across the upstream edges of the linings ($x=0$ plane). While the transverse vortex velocity turns from negative to positive during the passage of the vortex across the lined portion of the duct, the longitudinal vortex velocity remains higher than the original speed of the vortex throughout the interaction period. Again, the more pressure releasing the lining is, the higher the vortex velocity amplitude resulted. According to Eqs. (25) and (28), such higher vortex velocity, especially its transverse component, will imply stronger sound radiation.

The vortex accelerations contain high frequency components, as shown in Figs. 2(d) and 2(e). The time variations in the far field acoustic pressures shown in Fig. 2(f) follow closely those of the transverse vortex velocities [Fig. 2(c)], suggesting that the unsteady transverse vortex motion is the

major mechanism of sound radiation for $L=1$ and $y_{oi}=0.2$. The small amplitude fluctuations embedded in the far field pressure fluctuations are due to the terms $\dot{A}_n$'s and $\dot{B}_n$'s, which reflect the pressure fluctuations on the surfaces of the porous materials and are related to the acceleration of the vortex [cf. Eqs. (14) and (15)]. The results for the cases with $L=1$ and $y_{oi}=0.3$ are very similar to those shown in Fig. 2, but with smaller amplitudes. They are therefore not presented. The small amplitude fluctuations in the far field pressure for $L=1$ and $y_{oi}=0.3$ are too weak to be significant in the overall acoustic radiation. Such kind of small fluctuations is not observed in the flat plate case of Lau and Tang.[18] The presence of the upper duct wall results in non-monotonic longitudinal and transverse variations in the flow field with height in the lined duct section and thus the wrangling observed in Fig. 2.

It can be concluded that the pressure releasing effect of the porous linings, which is uneven on the upper and lower sides of the vortex due to the vortex height, results in a downward force on the fluid which is larger than that experienced by the vortex in the rigid wall section of the duct. This force causes the vortex to move downward and is only partially compensated by the increase in the vortex force[26] as the vortex speed increases. The vortex then accelerates downward until various forces are balanced. The vortex starts going upward under the effect of the downstream rigid duct wall after that. This transverse vortex motion results in a longitudinal vortex force which creates a longitudinal push to the fluid, which propagates into the far field and becomes sound. Such pushing is a plane dipole source. Sound generated from fluctuating vortex forces is also observed in the duct exhaust configuration of Cannell and Ffowcs Williams.[11]

The period of interaction between the vortex and the porous linings increases with L. Figure 3 summarizes the inviscid vortex dynamics and the sound radiation for $L=2$ and $y_{oi}=0.2$. While many of the essential features of Fig. 3 follow those shown in Fig. 2, the longer lengths of the linings result in stronger high frequency fluctuations in the vortex velocities and accelerations. For smaller h and/or larger η, pressure pulses are observed at the instants the vortex moves into and out of the lined duct section (the $x=0$ and $x=L$ planes, respectively). When the porous linings become more pressure releasing, the rates of change in A_n and B_n become dominant in the far field sound radiation. These rates of change are directly related to the vortex accelerations, such that the time fluctuation of far field sound pressure resembles those of the vortex accelerations instead of that of the transverse vortex velocity. Since it is not practical to have $h>1$ and the effect of the thickness of the porous lining on the vortex dynamics has been found to be more or less independent of h for $h>0.8$, the results with $h \geq 1$ are not discussed.

B. Combined effects of R_f and η

The flow resistance inside the lattice of the porous material is pressure-supporting. Large flow resistance therefore will produce an effect similar to large η in principle. Figure

J. Acoust. Soc. Am., Vol. 126, No. 3, September 2009

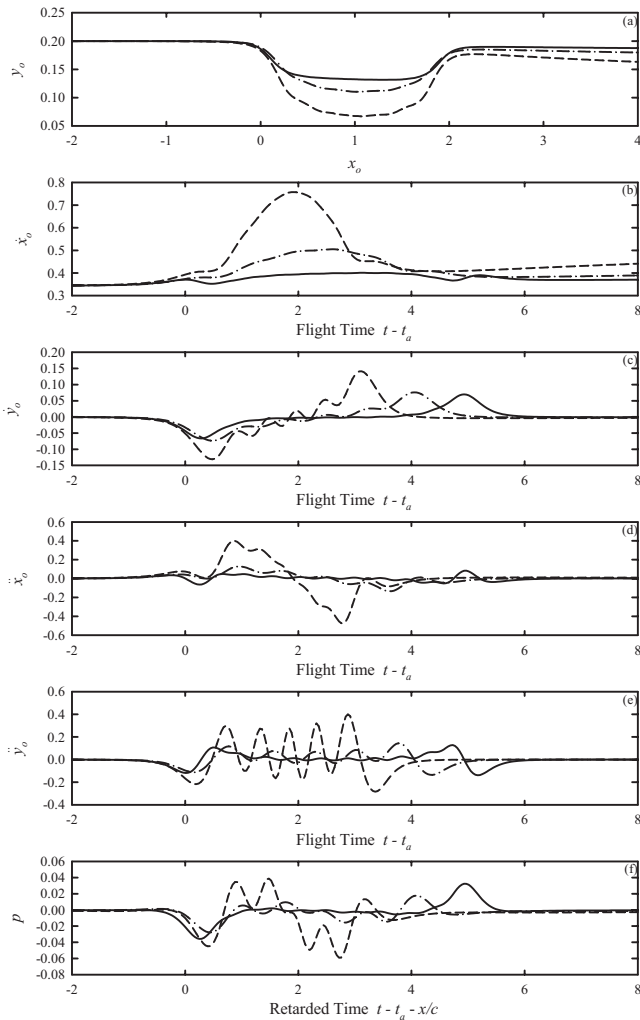S. K. Tang and C. K. Lau: Duct vortex sound   1009

FIG. 3. Effects of pressure-releasing linings on vortex dynamics and sound generation under inviscid condition for $L=2$ and $y_{oi}=0.2$. (a) Vortex path, (b) longitudinal velocity, (c) transverse velocity, (d) longitudinal acceleration, (e) transverse acceleration, and (f) far field sound pressure. ——: $h=0.2$, $\eta=3$; – – –: $h=0.8$, $\eta=3$; and –·–: $h=0.8$, $\eta=5$.

FIG. 4. Effects of R_f on vortex dynamics and sound generation for $L=1$, $y_{oi}=0.2$, $h=0.2$, and $\eta=3$. (a) Vortex path, (b) longitudinal velocity, (c) transverse velocity, (d) longitudinal acceleration, (e) transverse acceleration, and (f) far field sound pressure. ——: $R_f=0.5$; – – –: $R_f=3$; –·–: $R_f=7$; –··–: $R_f=30$; and ·········: $R_f=100$.

4 illustrates the vortex dynamics and the far field sound radiation for $y_{oi}=0.2$, $h=0.2$, $L=1$, and $\eta=3$ with increasing R_f. For small R_f, the pressure-releasing effect of the lining dominates and the vortex first bends toward the lower porous lining and then moves upward as it leaves the lined duct section under the pressure-supporting effect of the downstream rigid duct walls [Fig. 4(a)]. However, when R_f increases, the transverse velocity of the vortex is significantly reduced, as shown in Fig. 4(c). The vortex continues to move downward as it accelerates toward the end of the porous linings. The action time of the pressure-supporting downstream rigid duct wall is insufficient to pull the vortex up and can only result in producing a short duration of significant vortex acceleration when the vortex leaves the lined section [Figs. 4(d) and 4(e)]. Further increase in R_f makes the porous linings more pressure-supporting so that the bending of the vortex path, and thus the sound radiation [Fig. 4(f)], becomes less and less significant.

The far field sound time fluctuation patterns illustrated in Fig. 4(f) suggest that the transverse vortex velocity is not the major sound generation mechanism in the presence of a
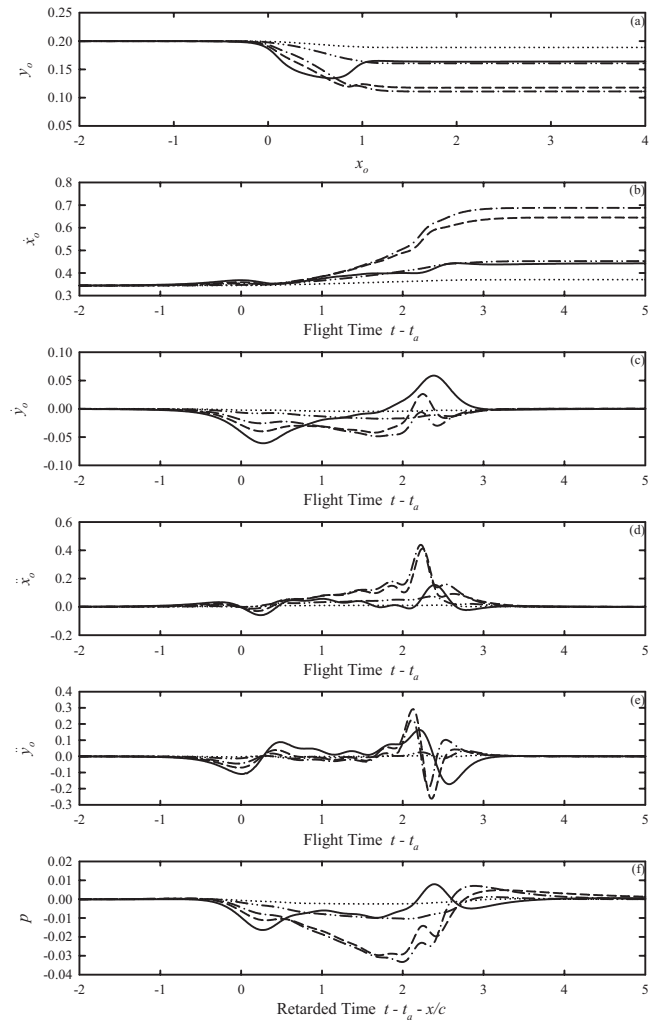
non-vanishing R_f. Strong sound energy radiation is observed within the range $3<R_f<10$ while the strongest radiation takes place when the vortex leaves the lined duct section. The rates of changes in the mode amplitudes A_n and B_n, which control the pressure fluctuations on the porous lining surfaces, play a role at least as significant as the transverse vortex velocity. One can also observe that the amplitude of the sound generated within this R_f range is greater than that for the inviscid cases. The increase in h results in strong pressure-releasing porous linings and thus deeper vortex path bending and stronger sound radiation at a fixed R_f. The opposite is observed when η is increased. The strongest sound radiation is still found within the same R_f range, and the instants of strongest sound radiation remain unchanged. These results are expected and thus are not presented.

The increase in the length of the lined section to $L=2$ gives rise to more severe vortex path bending toward the lower porous surface, as shown in Fig. 5(a). The prolonged interaction between the vortex and the porous linings at increased L results in higher vortex velocities especially when the vortex is close to the end of the lined section [Figs. 5(b)
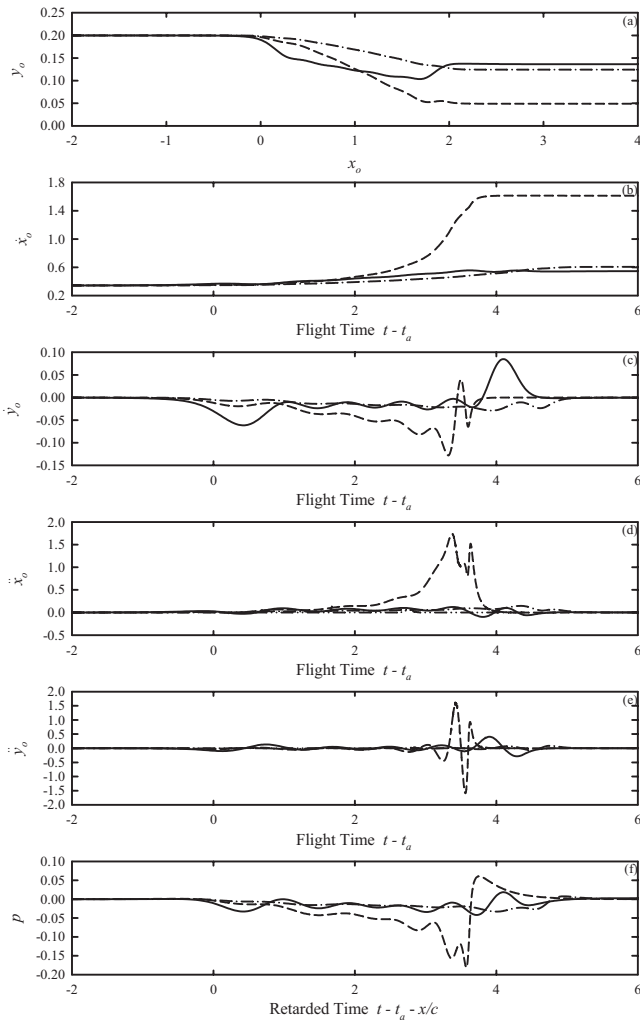
S. K. Tang and C. K. Lau: Duct vortex sound

FIG. 5. Effects of R_f on vortex dynamics and sound generation for $L=2$, $y_{oi}=0.2$, and $\eta=3$. (a) Vortex path, (b) longitudinal velocity, (c) transverse velocity, (d) longitudinal acceleration, (e) transverse acceleration, and (f) far field sound pressure. ——: $R_f=0.5$, $h=0.2$; $-$ $-$ $-$: $R_f=10$, $h=0.2$; and $-\cdot-$: $R_f=30$, $h=0.2$.
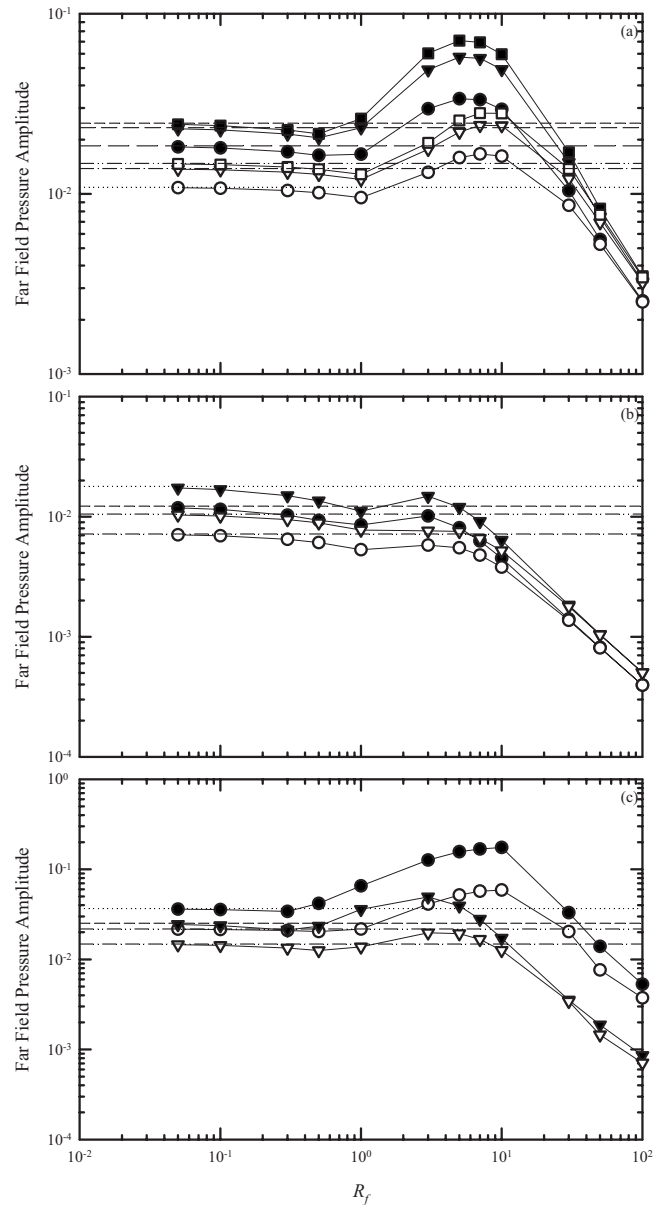

FIG. 6. Far field sound pressure amplitude under different combinations of system parameters. (a) $L=1$, $y_{oi}=0.2$, ●: $h=0.2$; ▼: $h=0.4$; ■: $h=0.8$; ----: $h=0.8$, $\eta=3$, $R_f=0$; $-$ $-$ $-$: $h=0.4$, $\eta=3$, $R_f=0$; $-$ $-$ $-$: $h=0.2$, $\eta=3$, $R_f=0$; $\cdots\cdots\cdots$: $h=0.2$, $\eta=5$, $R_f=0$; $-\cdot-$: $h=0.4$, $\eta=5$, $R_f=0$; and $-\cdots-$: $h=0.8$, $\eta=5$, $R_f=0$. (b) $L=1$, $y_{oi}=0.3$, ●: $h=0.2$; ▼: $h=0.4$; -----: $h=0.2$, $\eta=3$, $R_f=0$; $\cdots\cdots\cdots$: $h=0.4$, $\eta=3$, $R_f=0$; $-\cdot-$: $h=0.2$, $\eta=5$, $R_f=0$; and $-\cdots-$: $h=0.4$, $\eta=5$, $R_f=0$. (c) $L=2$, ●: $y_{oi}=0.2$, $h=0.2$; ▼: $y_{oi}=0.3$, $h=0.2$. ----: $y_{oi}=0.3$, $h=0.2$, $\eta=3$, $R_f=0$; $\cdots\cdots\cdots$: $y_{oi}=0.2$, $h=0.2$, $\eta=3$, $R_f=0$; $-\cdots-$: $y_{oi}=0.3$, $h=0.2$, $\eta=5$, $R_f=0$; and $-\cdots-$: $y_{oi}=0.2$, $h=0.2$, $\eta=5$, $R_f=0$. Closed symbols for $\eta=3$; open symbols for $\eta=5$.

and 5(c)]. Together with the higher vortex acceleration and deceleration near the instant at which the vortex leaves the lined section under the pressure-supporting effect of the rigid wall, stronger sound radiation is observed [Figs. 5(d)–5(f)]. The increase in the thickness of the porous linings results in stronger pressure-releasing effect, leading to higher vortex accelerations. Stronger sound radiation can then be expected from the results discussed previously in relation to Fig. 3. At $h=0.8$, the amplitude of the far field pressure is about seven times that at $h=0.2$ with the same initial vortex conditions for $R_f=10$ (not shown here). Other features observed in Fig. 5 are inline with those associated in Fig. 4 and thus are not discussed further.

Figure 6 summarizes the amplitude of the far field pressure generated under various combinations of the parameters studied. The horizontal lines represent the corresponding values for the perfectly inviscid case ($R_f=0$). The increase in h or a decrease in η will produce a louder sound because of the strong pressure-releasing effect of the porous lining which is expected.

For $y_{oi}=0.2$ and $L=1$, it can be observed that the slight

increase in R_f from the vanishing value results in a very small drop of the pressure amplitude below that of the corresponding inviscid case [Fig. 6(a)]. For $1<R_f<25$, louder sound than that created in the inviscid case is observed for $\eta=3$. The maximum sound pressure appears at $R_f \sim 6$. The maximum sound pressure level increases by 5 dB above that in the inviscid case for $h=0.2$ and by as high as 9 dB for $h=0.8$. Further increase in R_f results in more pressure-supporting porous linings. This effect overcomes the pressure-releasing effect of η, resulting in the continuous drop of sound pressure as R_f increases behind 30.

The range of R_f for sound amplification is slightly reduced when η increases from 3 to 5, as shown in Fig. 6(a). The increases in sound pressure levels above the inviscid value are ~4 and ~6 dB for $h=0.2$ and 0.8, respectively. This trend suggests that no sound amplification will be achieved when η is increased further or when the lining becomes more and more pressure-supporting.

When the initial vortex height y_{oi} is increased, the effects of the linings on the vortex dynamics are less severe than those in the case when the vortex moves closer to the lower lining. The increase in R_f then results in weaker sound generation, as shown in Fig. 6(b). One should note that the lower lining in this case is less pressure-releasing as experienced by the vortex and thus the results in Fig. 6(b) are actually following the trend illustrated in Fig. 6(a).

The increase in L to 2 prolongs the active interaction period between the vortex and the linings. The magnitude of the far field sound pressure is increased, as indicated previously in Figs. 4 and 5. The range of R_f for sound amplification is large, as shown in Fig. 6(c). The increase in the far field sound pressure level is also impressive. For $y_{oi}=0.2$, $h=0.2$, and $\eta=3$, the maximum sound pressure level created is ~14 dB higher than both resulted in the inviscid situation and in the corresponding $L=1$ case. The increase in h to 0.8 results in an ~17 dB higher in the maximum sound pressure level than the corresponding $h=0.2$ case (not shown here). The increase in either y_{oi} or η reduces the far field sound amplitude as expected. In addition, one can observe from Fig. 6(c) that the value of R_f for maximum sound amplitude decreases as y_{oi} increases, but does not appear to depend much on η.

The variations in the radiated acoustical energy per unit spanwise length E with the present system parameters follow very closely those of the sound pressure amplitudes, as shown in Fig. 7. This is expected as a plane wave is produced at the far field so that

$$E = 2\int_{-\infty}^{\infty}\int_{0}^{1}(p^2/c)dydt = \frac{2}{c}\int_{-\infty}^{\infty}p^2dt, \qquad (29)$$

and E is normalized by $\rho\Gamma^2$. However, the range of R_f for stronger acoustical energy radiation than the inviscid case, if there is, is wider than that for the sound pressure amplification shown in Fig. 6. This is because of the longer durations of active sound radiation than those in the inviscid cases. For $y_{oi}=0.2$, $h=0.8$, and $\eta=3$, the highest increase in the energy radiation is about 18 dB above that of the corresponding inviscid case, which is significantly higher than the 9 dB increase in the sound pressure level discussed before, and it occurs at $R_f\sim5$ [Fig. 7(a)].

Figure 7(b) illustrates that lower energy radiation than that in the inviscid case is still observed for $y_{oi}=0.3$ when the lower porous lining effect is reduced. However, the percentage energy reduction is less than that for the sound pressure amplitude shown in Fig. 6(b). The longer lining length results in stronger acoustical energy radiation than that in the inviscid case even at small R_f [Fig. 7(c)]. Again, the percentage increase in the acoustical energy radiation is higher than that of the sound pressure amplitude.
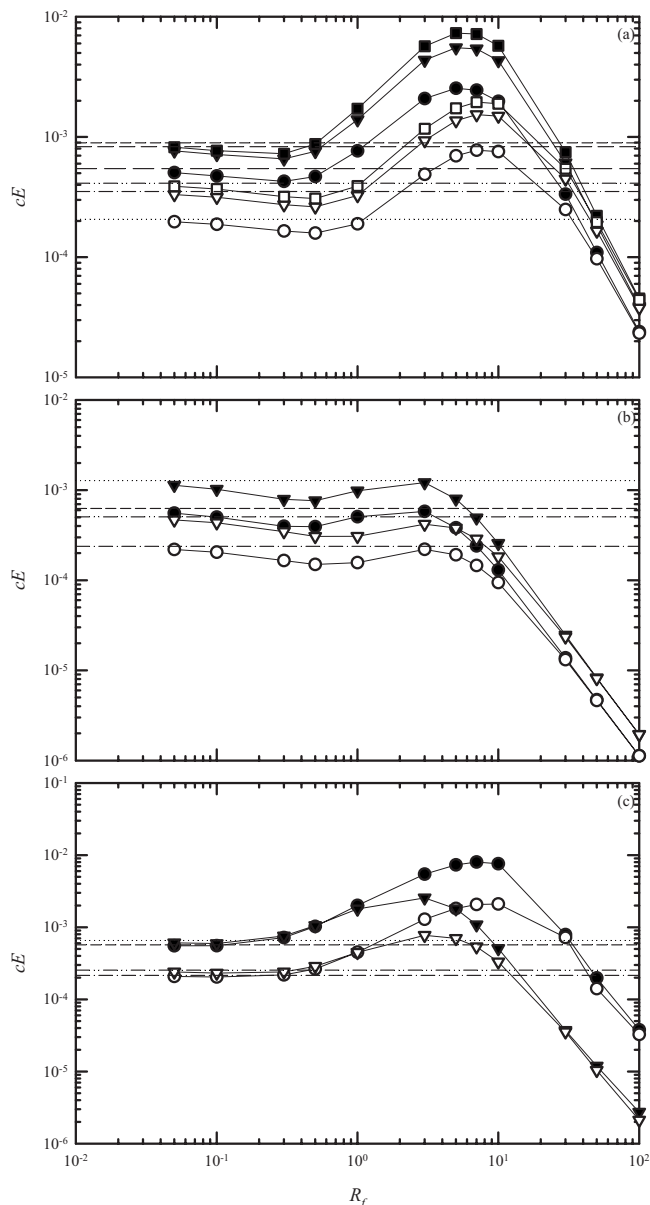

FIG. 7. Acoustical energy radiated per unit spanwise length under different combinations of system parameters. (a) $L=1$, $y_{oi}=0.2$; (b) $L=1$, $y_{oi}=0.3$; and (c) $L=2$. Legends: same as those for Fig. 6.

IV. CONCLUSIONS

The sound generated by the unsteady motion of a vortex moving across a lined duct section is investigated theoretically in the present study. The streamfunctions inside the flow field and inside the porous linings derived in terms of infinite series consist of modes with time varying magnitudes. The standard fourth order Runge–Kutta method was used to solve the coupled vortex dynamics equations numerically. The method of matched asymptotic expansion was applied to determine the time variation in the far field pressure so generated. The vortex was set at large distance upstream of the lined duct section initially and was located below the duct centerline to ensure its downstream propagation.

For a perfectly inviscid fluid, the pressure-releasing effect of the porous linings results in a downward transverse motion of the vortex. The longitudinal speed of the vortex

increases. The transverse vortex motion is the major sound generation mechanism when the lined section is not too long. As this length increases, the effects of the rates of change in the mode magnitudes, which affect directly the pressure on the lining surfaces and the vortex accelerations, become more significant in the sound radiation process. The increase in the effective fluid density inside the linings weakens the sound radiation.

The flow resistance inside the porous linings is pressure-supporting. It tends to increase the duration of active interaction between the vortex and the porous linings, resulting in stronger sound radiation after it has increased to an extent after which it overrides the pressure-releasing effect of the effective fluid density. However, its pressure-supporting property eventually attenuates the unsteady motion of the vortex and thus weakens the sound generation as it increases further. In the presence of a non-vanishing flow resistance, the rates of change in the mode magnitudes, which are directly related to the vortex accelerations, and the transverse vortex motions are of comparable importance in the radiation of sound. The prolonged interaction between the vortex and the linings in the presence of flow resistance results in greater/lower percentage increase/reduction in the acoustical energy radiated than that in the sound pressure amplification/attenuation.

ACKNOWLEDGMENT

APPENDIX: G_1, G_2, H_1, H_2, AND THE RATES OF CHANGE OF MODE MAGNITUDES

The expressions for G_1, G_2, H_1, and H_2 can be obtained by solving Eqs. (8), (11), and (12). It is straight-forward to show that

$$G_1 = -\frac{e^{ikx_o}}{2|k|}\frac{\sinh(|k|(1-y_o))}{\sinh(|k|)}$$
$$+\sum_{n=1}^{\infty}\frac{(-1)^n e^{ikL}-1}{k^2-\alpha_n^2}\frac{A_n e^{|k|}-B_n}{2\sinh(|k|)}\alpha_n e^{\alpha_n h}\sinh(\alpha_n h),$$

$$G_2 = \frac{e^{ikx_o}}{2|k|}\frac{\sinh(|k|(1-y_o))}{\sinh(|k|)}$$
$$-\sum_{n=1}^{\infty}\frac{(-1)^n e^{ikL}-1}{k^2-\alpha_n^2}\frac{A_n e^{-|k|}-B_n}{2\sinh(|k|)}\alpha_n e^{\alpha_n h}\sinh(\alpha_n h),$$

$$H_1 = \frac{e^{ikx_o}}{2|k|}\frac{\sinh(|k|y_o)}{\sinh(|k|)}e^{|k|}$$
$$+\sum_{n=1}^{\infty}\frac{(-1)^n e^{ikL}-1}{k^2-\alpha_n^2}\frac{A_n e^{|k|}-B_n}{2\sinh(|k|)}\alpha_n e^{\alpha_n(1+h)}\sinh(\alpha_n h),$$

$$H_2 = -\frac{e^{ikx_o}}{2|k|}\frac{\sinh(|k|y_o)}{\sinh(|k|)}e^{-|k|}$$
$$-\sum_{n=1}^{\infty}\frac{(-1)^n e^{ikL}-1}{k^2-\alpha_n^2}\frac{A_n e^{-|k|}-B_n}{2\sinh(|k|)}\alpha_n e^{\alpha_n(1+h)}\sinh(\alpha_n h).$$
(A1)

It can also be shown from Eqs. (17) and (18) that

$$\int_0^L\int_{-\infty}^{\infty}|k|(\dot{G}_2-\dot{G}_1)e^{-ikx}dk\sin(\alpha_m x)dx$$
$$= \pi(\eta\dot{A}_m+R_f A_m)\alpha_m e^{\alpha_m h}\cosh(\alpha_m h),$$
(A2)

and

$$\int_0^L\int_{-\infty}^{\infty}|k|(\dot{H}_2 e^{|k|}-\dot{H}_1 e^{-|k|})e^{-ikx}dk\sin(\alpha_m x)dx$$
$$= -\pi(\eta\dot{B}_m+R_f B_m)\alpha_m e^{\alpha_m(1+h)}\cosh(\alpha_m h).$$
(A3)

With the expressions in Eq. (A1), Eqs. (A2) and (A3) can be re-written into the forms

$$-X_{A,m}\dot{x}_o+Y_{A,m}\dot{y}_o+\sum_{n=1}^{\infty}\beta_{mn}\dot{A}_n\alpha_n e^{\alpha_n h}\sinh(\alpha_n h)$$
$$+\sum_{n=1}^{\infty}\gamma_{mn}\dot{B}_n\alpha_n e^{\alpha_n(1+h)}\sinh(\alpha_n h)$$
$$= \frac{L}{2}(\eta\dot{A}_m+R_f A_m)\alpha_m e^{\alpha_m h}\cosh(\alpha_m h)$$
(A4)

and

$$-X_{B,m}\dot{x}_o+Y_{B,m}\dot{y}_o-\sum_{n=1}^{\infty}\gamma_{mn}\dot{A}_n\alpha_n e^{\alpha_n h}\sinh(\alpha_n h)$$
$$+\sum_{n=1}^{\infty}\beta_{mn}\dot{B}_n\alpha_n e^{\alpha_n(1+h)}\sinh(\alpha_n h)$$
$$= -\frac{L}{2}(\eta\dot{B}_m+R_f B_m)\alpha_m e^{\alpha_m(1+h)}\cosh(\alpha_m h),$$
(A5)

respectively, where

$$\beta_{mn} = -\frac{1}{\pi}\int_0^{\infty}\frac{k\alpha_m\coth(k)}{(k^2-\alpha_n^2)(k^2-\alpha_m^2)}$$
$$\times\{(-1)^{m+n}-[(-1)^n+(-1)^m]\cos(kL)+1\}dk,$$

$$\gamma_{mn} = \frac{1}{\pi}\int_0^{\infty}\frac{k\alpha_m}{(k^2-\alpha_n^2)(k^2-\alpha_m^2)\sinh(k)}$$
$$\times\{(-1)^{m+n}-[(-1)^n+(-1)^m]\cos(kL)+1\}dk,$$

$$X_{A,m} = -\frac{1}{\pi}\int_0^{\infty}\frac{k\alpha_m\sinh(k(1-y_o))}{(k^2-\alpha_m^2)\sinh(k)}$$
$$\times[(-1)^m\sin(k(L-x_o))+\sin(kx_o)]dk,$$

$$Y_{A,m} = -\frac{1}{\pi}\int_0^\infty \frac{k\alpha_m \cosh(k(1-y_o))}{(k^2-\alpha_m^2)\sinh(k)}$$
$$\times[(-1)^m \cos(k(L-x_o)) - \cos(kx_o)]dk,$$

$$X_{B,m} = \frac{1}{\pi}\int_0^\infty \frac{k\alpha_m \sinh(ky_o)}{(k^2-\alpha_m^2)\sinh(k)}$$
$$\times[(-1)^m \sin(k(L-x_o)) + \sin(kx_o)]dk,$$

and

$$Y_{B,m} = -\frac{1}{\pi}\int_0^\infty \frac{k\alpha_m \cosh(ky_o)}{(k^2-\alpha_m^2)\sinh(k)}$$
$$\times[(-1)^m \cos(k(L-x_o)) - \cos(kx_o)]dk.$$

It can be noted that $\beta_{mn} = \gamma_{mn} = 0$ if $(m+n)$ is an odd integer. The rates of change in the mode magnitudes can then be obtained by simple matrix operation as in Ref. 18 once A_n, B_n, and the vortex velocity are known.

[1]H. G. Davies and J. E. Ffowcs Williams, "Aerodynamic sound generation in a pipe," J. Fluid Mech. **32**, 765–778 (1968).
[2]N. Curle, "The influence of solid boundaries upon aerodynamic sound," Proc. R. Soc. London, Ser. A **231**, 505–514 (1955).
[3]C. M. Harris, *Handbook of Noise Control* (McGraw-Hill, New York, 1979).
[4]A. Cummings and I.-J. Chang, "Sound attenuation of a finite length dissipative flow duct silencer with internal mean flow in the absorbent," J. Sound Vib. **127**, 1–17 (1988).
[5]K. S. Peat and K. L. Rathi, "A finite element analysis of the convected acoustic wave motion in dissipative silencers," J. Sound Vib. **184**, 529–545 (1995).
[6]A. Selamat, I. J. Lee, and N. T. Huff, "Acoustic attenuation of hybrid silencers," J. Sound Vib. **262**, 509–527 (2003).
[7]J. E. Ffowcs Williams, "The acoustics of turbulence near sound-absorbent liners," J. Fluid Mech. **51**, 737–749 (1972).
[8]M. C. Quinn and M. S. Howe, "On the production and absorption of sound by lossless liners in the presence of mean flow," J. Sound Vib. **97**, 1–9 (1984).
[9]L. M. Milne-Thomson, *Theoretical Hydrodynamics* (The University Press, Glasgow, UK, 1968).
[10]A. Powell, "Theory of vortex sound," J. Acoust. Soc. Am. **36**, 177–195 (1964).
[11]P. Cannell and J. E. Ffowcs Williams, "Radiation from line vortex filaments exhausting from a two-dimensional semi-infinite duct," J. Fluid Mech. **58**, 65–80 (1973).
[12]D. G. Crighton, "Radiation from vortex filament motion near a half plane," J. Fluid Mech. **51**, 357–362 (1972).
[13]F. Obermeier, "The influence of solid bodies on low Mach number vortex sound," J. Sound Vib. **72**, 39–49 (1980).
[14]M. S. Howe, *Theory of Vortex Sound* (Cambridge University Press, Cambridge, 2003).
[15]S. K. Tang, "Effects of porous boundaries on the dynamics of an inviscid vortex filament," Q. J. Mech. Appl. Math. **54**, 65–84 (2001).
[16]S. K. Tang and C. K. Lau, "Vortex sound in the presence of a wedge with inhomogeneous surface flow impedance," J. Sound Vib. **281**, 1077–1091 (2005).
[17]C. K. Lau and S. K. Tang, "Sound generated by vortices in the presence of a porous half-cylinder mounted on a rigid plane," J. Acoust. Soc. Am. **119**, 2084–2095 (2006).
[18]C. K. Lau and S. K. Tang, "Vortex sound under the influence of a piecewise porous material on an infinite rigid plane," J. Acoust. Soc. Am. **122**, 2542–2550 (2007).
[19]P. M. Morse and K. U. Ingard, *Theoretical Acoustics* (McGraw-Hill, New York, 1968).
[20]I. S. Gradshteyn and I. M. Ryzhik, *Tables of Integrals, Series and Products* (Academic, New York, 1965).
[21]R. V. Churchill and J. W. Brown, *Complex Variables and Applications* (McGraw-Hill, New York, 1990).
[22]M. Van Dyke, *Perturbation Methods in Fluid Mechanics* (Parabolic, Stanford, CA, 1975).
[23]J. E. Ffowcs Williams and D. J. Lovely, "Sound radiation into uniformly flowing fluid by compact surface vibration," J. Sound Vib. **71**, 689–700 (1975).
[24]S. K. Tang, R. C. K. Leung, and R. M. C. So, "Vortex sound due to a flexible boundary backed by a cavity in a low Mach number mean flow," J. Acoust. Soc. Am. **121**, 1345–1352 (2007).
[25]M. S. Howe, "A note on the interaction of unsteady flow with an acoustic liner," J. Sound Vib. **63**, 429–436 (1979).
[26]P. G. Saffman, *Vortex Dynamics* (Cambridge University Press, Cambridge, 1992).